Biotechnology Journal

DOI 10.1002/biot.201200393

Biotechnol. J. 2013, 8, 1058–1069

Research Article

Metabolic gradients as key regulators in zonation of tumor energy metabolism: A tissue-scale model-based study

Matthias König, Hermann-Georg Holzhütter and Nikolaus Berndt

Institute of Biochemistry, University Medicine Charité Berlin, Berlin, Germany

Characteristics of many tumor types are the reprogramming of metabolism and the occurrence of regional hypoxia. In this work, we investigated the hypothesis that metabolic reprogramming in combination with metabolic zonation of cellular energy metabolism are important factors in promotion of the growth capacity of solid tumors. A tissue-scale model of the two main ATP delivering pathways, glycolysis (GLY) and oxidative phosphorylation (OXP), was used to simulate the energy metabolism within solid tumors under various metabolic strategies. Remarkably, despite the high diversity in the usage of glucose, lactate and oxygen in various spatial regions, the tumor as a whole clearly displays the hallmark of the so-called Warburg effect, i.e. a high rate of glucose consumption and lactate production in the presence of sufficiently high levels of oxygen. Our simulations suggest that an increase in GLY capacity and concomitant decrease in OXP capacity from the periphery towards the center of the tumor improves the availability of oxygen to pericentral tumor cells. The found relationship between the regional oxygen level and the relative share of GLY and OXP capacities supports the view that metabolite availability functions as key regulator of tumor energy metabolism.

Received	07 DEC 2012
Revised	04 FEB 2013
Accepted	15 APR 2013
Accepted article online	16 APR 2013

Supporting information available online

Keywords: Hypoxia · Metabolic reprogramming · Metabolic zonation · Oxygen · Warburg effect

1 Introduction

Metabolic zonation designates the finding that homotypic cells in a tissue may comprise significant differences in the capacity of specific metabolic pathways depending on their local access to nutrients and oxygen. Well-studied examples are hepatocytes or kidney cells, which may alternatively operate as glucose producers in well-oxygenated regions (aerobic) of the tissue (periportal, respectively near-cortex proximal) or glucose consumers in poorly oxygenated (hypoxic) regions (perivenious) [1–3]. These striking regional differences in the capacity of gluconeogenesis and glycolysis (GLY) are mainly due to differences in the expression of the underlying key enzymes, transporters and receptors, resulting in different functional capacities, which are either stably established during tissue development and regeneration or transiently induced by changes in the environmental conditions like available oxygen [4, 5].

A hallmark of many tumor types is the reprogramming of the energy metabolism [6], resulting in an extraordinarily high demand for glucose even under aerobic conditions (the so-called Warburg effect) with a substantial part of glucose being converted into lactate. Another key characteristic of most tumors is regional hypoxia [7, 8] considered a key regulatory factor in tumor growth [7]. Regional hypoxia in tumors is a consequence of diffusion limitations in combination with altered and non-functional tumor microvasculature [9, 10]. This results in the coexistence of aerobic regions close to supporting blood vessels and hypoxic or even anoxic regions in larger distances from the blood supply [11]. In tumor microspheroids, a lab model of solid tumors that receive their supply of oxygen and nutrients only through diffusion from the outer cell layer (periphery) to the center, one may distinguish with increasing distance from the periphery between an outer viable rim, consisting of proliferating

Correspondence: Matthias König, Institute of Biochemistry, University Medicine Charité Berlin, Virchowweg 6, 10117 Berlin, Germany
E-mail: matthias.koenig@charite.de

Abbreviations: HIF, hypoxia-inducible factor; **GLY**, glycolysis; **pO_2**, partial pressure of oxygen; **OXP**, oxidative phosphorylation; **TCA**, tricarboxylic acid

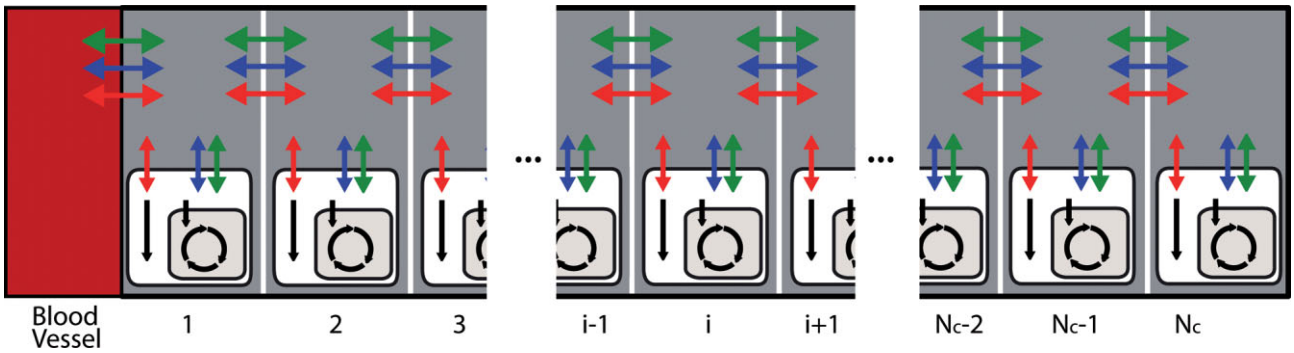

Figure 1. Tissue-scale model of tumor metabolism. Overview of the multi-scale model of tumor metabolism integrating diffusion-based transport of metabolites in the extracellular space (grey) with detailed kinetic models of energy metabolism on the cellular level (Fig. 2). Exchangeable metabolites between the cells and the extracellular space are glucose (red), lactate (green) and oxygen (blue). The tumor is supplied with nutrients and oxygen via the nearest blood vessel.

cells, an intermediary region of quiescent and hypoxic cells, and an inner necrotic core [12, 13]. The relative share of GLY and oxidative phosphorylation (OXP) in the total energy production of tumor cells can be adapted to varying oxygen levels via transcriptional regulation of key metabolic genes through oxygen-sensitive transcription factors like hypoxia-inducible factor-1 (HIF-1) [8, 11, 14]. HIF-1 may up-regulate the expression level of glycolytic enzymes [11, 14, 15] and can down-regulate OXP via multiple mechanisms as, for example reducing the activity of pyruvate dehydrogenase via transactivation of pyruvate dehydrogenase kinase I (PDK1) [16, 17] or reducing the number of mitochondria per cell due to the induction of MAX interactor 1 (MXI1) [18]. These HIF-dependent changes result in a zonated tumor energy metabolism characterized by varying metabolic capacities of GLY and OXP with changing oxygen availability.

In this work, we address the problem whether zonation of the energy metabolism within a non-vascular tumor could serve as a means to promote its growth capacity. We used a detailed kinetic model of the cellular energy metabolism comprising the two central ATP delivering pathways, GLY and OXP, to simulate the energy metabolism of tumor cells at varying distance from the nearest blood supply and under different metabolic strategies. In this model, glucose, lactate and oxygen in the extracellular space were considered diffusively exchangeable between adjacent spatial layers.

2 Methods

The presented model is a tissue-scale model of tumor metabolism applicable to small avascular tumors, microregions of larger tumors and tumor spheroids having access to nutrients in the blood (or in the medium) only through extracellular diffusion from the periphery to the center. The model integrates a diffusion-based model of metabolite transport in extracellular space with detailed kinetic models of single-cell energy metabolism (Fig. 1). Glucose, lactate and oxygen are exchanged between the supporting blood vessel and the tumor tissue and between cells and extracellular space. The sub-system of cellular metabolism comprises GLY, tricarboxylic acid cycle (TCA cycle) and OXP (Fig. 2). The resulting integrative model is an ordinary differential equation (ODE) model coupling the rate equations of biochemical reactions and membrane transport processes with the diffusion equations for the extracellular substrates. Model parameters are given in Table 1, Supporting information, Supplement 1 or are specified in the main text together with the respective equations.

2.1 Diffusion in extracellular space

The diffusion of the metabolites glucose, lactate and oxygen in the tumor is modeled by subdividing the extracellular space into small compartments whereby the exchange of metabolites between neighboring compartments is governed by one-dimensional diffusion equations. The complete tissue model consists of N_c layers of cells ranging from the blood vessel to the tumor core with each cell having N_f associated extracellular compartments (i.e. $N_{ext} = N_c \cdot N_f$ extracellular compartments in total). With glc_{blood} denoting the glucose concentration in the blood, glc_{ext}^k denoting the glucose concentration in the extracellular compartment k and D^{glc} being the diffusion coefficient of glucose in the extracellular space, the diffusion rate of glucose in the k-th compartment is given by

$$v_{Diff}^{glc}(k) = \frac{D^{glc}}{(d_{ext})^2}\left(\frac{1}{2}glc_{ext}^{k-1} - glc_{ext}^{k} + \frac{1}{2}glc_{ext}^{k+1}\right)$$

$$\forall k = 2,\ldots,N_{ext}-1 \qquad (1)$$

$$v_{Diff}^{glc}(k=1) = \frac{D^{glc}}{(d_{ext})^2}\left(\frac{1}{2}glc_{blood} - glc_{ext}^{1} + \frac{1}{2}glc_{ext}^{2}\right) \qquad (2)$$

Biotechnol. J. 2013, 8, 1058–1069

Table 1. Geometrical model parameters and diffusion coefficients for tissue-scale model

Parameter	Value	Description	Reference
N_c	25	number of cells in tissue model with cells $i = 1,..., N_c$	
N_f	5	number of extracellular compartments per cell (discretization)	
N_{ext}	$N_c \cdot N_f$	number of extracellular compartments with compartments $k = 1,..., N_{ext}$	
D^{glc}	$400\frac{\mu m^2}{s}$	diffusion coefficient glucose	[37, 51]
D^{lac}	$230\frac{\mu m^2}{s}$	diffusion coefficient lactate (~70% glucose [52])	[53, 54]
D^{o2}	$1500\frac{\mu m^2}{s}$	diffusion coefficient oxygen	[55, 56]
d_{cell}	15 μm	diameter single cell	
d_{ext}	$\frac{d_{cell}}{N_f}$	diameter extracellular compartment	
f_{ext}	0.3	extracellular volume fraction	[58]
V_{cell}	$(d_{cell})^3$	volume single cell	
V_{ext}	$f_{ext}\frac{V_{cell}}{N_f}$	volume single extracellular compartment	
N_{xin}	78	number of cellular concentrations single cell	
N_{xout}	3	number of extracellular concentrations	

$$v_{Diff}^{glc}(k = N_{ext}) = \frac{D^{glc}}{\left(d_{ext}\right)^2}\left(\frac{1}{2}glc_{ext}^{N_{ext}-1} - glc_{ext}^{N_{ext}}\right) \quad (3)$$

The diffusion rates of lactate $v_{Diff}^{lac}(k)$ and oxygen $v_{Diff}^{o2}(k)$ are calculated accordingly with blood concentrations as lac_{blood} and $o2_{blood}$, diffusion coefficients as D^{lac} and D^{o2}, and the concentrations in compartment k as lac_{ext}^k and $o2_{ext}^k$, respectively.

2.2 Kinetic model of cellular energy metabolism

The energy metabolism of a single tumor cell is described by a detailed kinetic model encompassing the pathways GLY, TCA cycle, and OXP and the compartments cytosol, mitochondrion and extracellular space. Well-characterized mathematical models for cancer GLY [19] have been published but no validated models of cancer metabolism comprising glycolysis, TCA cycle and OXP are currently available. Therefore, the kinetic equations for the enzymatic reactions and membrane transport processes were based on a model of energy metabolism for neuronal tissue [20] but without inclusion of tumor-specific isoforms (Fig. 2).

According to the model, ATP is produced in the glycolytic pathway (2 ATP per glucose) and in the presence of oxygen by mitochondrial OXP, which is exclusively fuelled by pyruvate that may either derive from glycolytic degradation of glucose or from lactate taken up from the extracellular space. The metabolic capacities of GLY and OXP were varied by scaling all reactions of the respective pathways. Experimental data for oxygen profiles, the dependency of the viable rim and oxygen consumption for mouse breast carcinoma spheroids (EMT6/Ro) [21, 22] were used to evaluate the respective strategies. All rate equations with the respective parameters and references are given in Supporting information, Supplement 1.

2.3 Integrative tissue model of energy metabolism

The diffusion model is coupled with the single-cell kinetic metabolic models via the exchange of glucose, lactate and oxygen between the cell $i = 1,\ldots N_c$ and the adjacent extracellular compartments $k = (i-1)\cdot N_f + 1,\ldots,i\cdot N_f$. The transport rates of glucose by the transporter GLUT, lactate by the transporter MCT and oxygen between extracellular space k and cell i are given by $glc_{ext}^k \rightarrow glc^i$: $v_{GLUT}(i, k)$, $o2_{ext}^k \rightarrow o2^i$: $v_{O2T}(i, k)$, and $lac_{ext}^k \rightarrow lac^i$: $v_{MCT}(i, k)$.

The concentration changes in the extracellular compartment k are the combination of diffusion transport and exchange with the adjacent cell i:

$$\frac{dglc_{ext}^k}{dt} = v_{Diff}^{glc}(k) - v_{GLUT}(i,k)\frac{V_{cell}}{V_{ext}} \quad (4)$$

$$\frac{do2_{ext}^k}{dt} = v_{Diff}^{o2}(k) - v_{O2T}(i,k)\frac{V_{cell}}{V_{ext}} \quad (5)$$

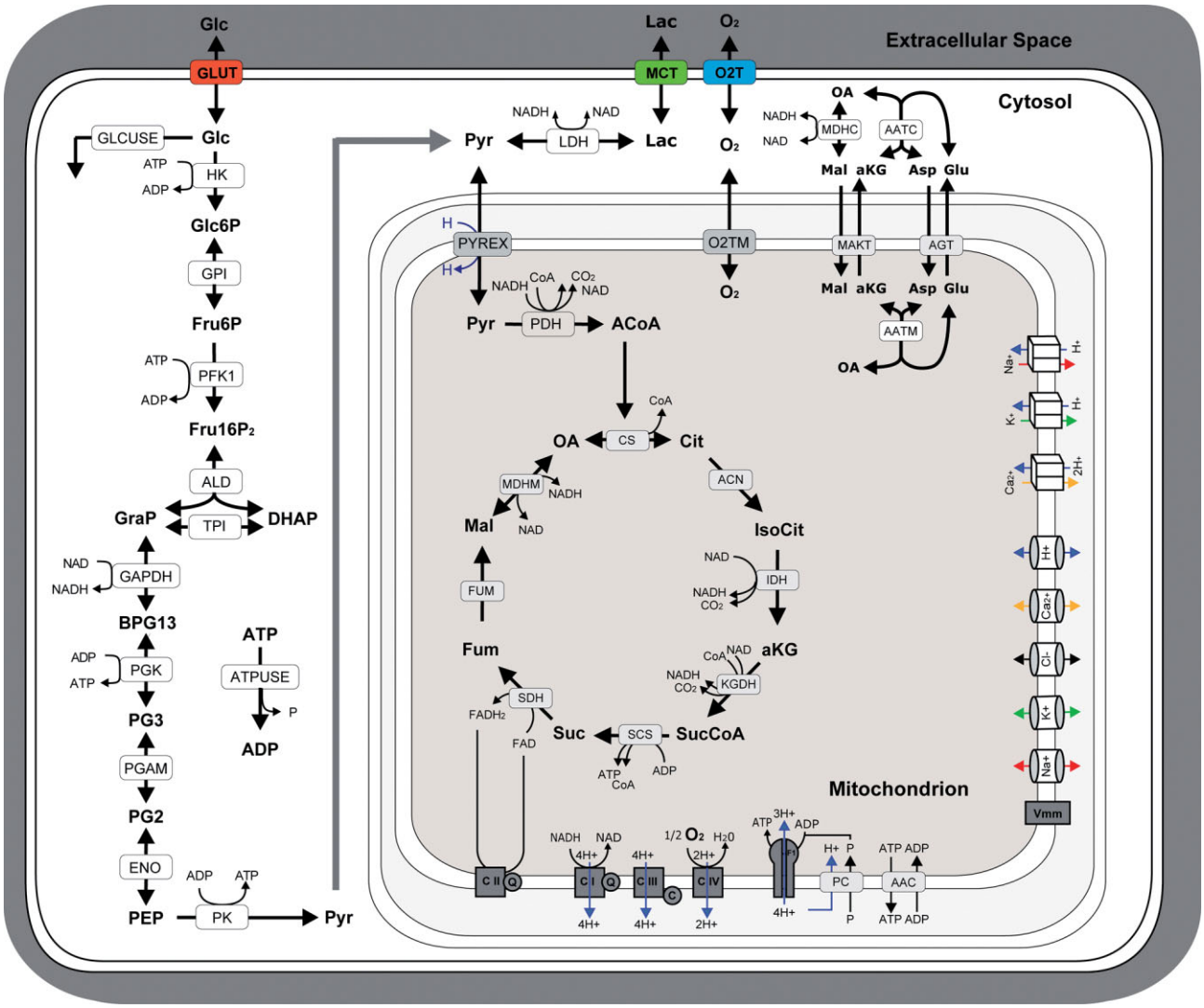

Figure 2. Single-cell energy metabolism. Overview of the detailed kinetic model of energy metabolism of the individual tumor cells comprising GLY, TCA cycle and OXP. The model is compartmentalized in cytosol, mitochondrion and extracellular space. The strategy of ATP production depends on the actual capacities of the individual cell for GLY Φ_{GLY} and OXP Φ_{OXP} as well as the available nutrients and oxygen. Glucose (red), lactate (green) and oxygen (blue) can be exchanged with the extracellular space. More detailed information is provided in Sect. 2 and Supporting information, Supplement 1. Reactions: AAC, ADP/ADP carrier; AATC, aspartate aminotransferase cytosol; AATM, aspartate aminotransferase mitochondrion; ACN, aconitase; AGT, aspartate/glutamate transport; ALD, aldolase; ATPUSE, ATP utilization; C I, complex I – NADH-coenzyme Q oxidoreductase; C II, complex II – succinate-Q oxidoreductase; C III, complex III – Q-cytochrome c oxidoreductase; C IV, complex IV - cytochrome c oxidase; CS, citrate synthase; ENO, enolase; F1, F_0F_1-ATPase/ATP-synthase; FUM, fumarase; GAPDH, glyceraldehyde 3-phosphate isomerase; GLUT, glucose transport; GLCUSE, glucose usage; GPI, glucose-phosphate isomerase; HK, hexokinase; IDH, isocitrate dehydrogenase; KGDH, α-ketoglutarate dehydrogenase; MAKT, malate/α-ketoglutarate transport; MCT, monocarboxylate transporter lactate; MDHM, malate dehydrogenase mitochondrion; MDHC, malate dehydrogenase cytosol; O2T, oxygen transport; O2TM, oxygen transport mitochondrion; PC, phosphate carrier; PDH, pyruvate dehydrogenase; PFK1, phospofructokinase 1; PGAM, phosphoglycerate mutase; PGK, phosphoglycerate kinase; PK, pyruvate kinase; PYREX, pyruvate exchanger; SCS, succinyl-CoA synthetase; SDH, succhinate dehydrogenase; TPI, triosephosphate isomerase. Ion channels and antiporter: $Ca^{2+}/2H^+$ antiporter, K^+/H^+ antiporter, Na^+/H^+ antiporter, Ca^{2+} channel, Cl^- channel, H^+ channel, K^+ channel, Na^+ channel; Vmm, mitochondrial membrane potential. Metabolites: ACoA, acetyl coenzyme A; ADP, adenosine diphosphate; aKG, α-ketoglutarate; Asp, aspartate; ATP, adenosine triphosphate; BPG13, 1,3-bisphosphoglycerate; C, cytochrome c; Cit, citrate; DHAP, dihydroxyacetone phosphate; Fru6P, fructose 6-phosphate; $Fru16P_2$, fructose 1,6-bisphosphate; Fum, fumarate; Glc, glucose; Glc6P, glucose 6-phosphate; Glu, glutamate; GraP, glyceraldehyde 3-phosphate; IsoCit, isocitrate; Lac, lactate; Mal, malate; NAD, nicotinamide adenine dinucleotide; O_2, oxygen; OA, oxaloacetate; P, phosphate; PEP, phosphoenolpyruvate; PG3, 3-phosphoglycerate; PG2, 2-phosphoglycerate; Pyr, pyruvate; Q, coenzyme Q; Suc, succhinate; SucCoA, succhinyl coenzyme A.

Biotechnol. J. 2013, 8, 1058–1069

$$\frac{dlac_{ext}^{k}}{dt} = v_{Diff}^{lac}(k) - v_{MCT}(i,k)\frac{V_{cell}}{V_{ext}} \quad (6)$$

The concentration changes in cell i are the combination of cellular metabolism and exchange with the adjacent extracellular volumes:

$$\frac{dglc^{i}}{dt} = \sum_{k=(i-1)N_f+1}^{i\cdot N_f} v_{GLUT}(i,k) - v_{HK}(i) \quad (7)$$

$$\frac{do2^{i}}{dt} = \sum_{k=(i-1)N_f+1}^{i\cdot N_f} v_{O2T}(i,k) - v_{O2TM}(i) \quad (8)$$

$$\frac{dlac^{i}}{dt} = -\sum_{k=(i-1)N_f+1}^{i\cdot N_f} v_{MCT}(i,k) + v_{LDH}(i) \quad (9)$$

All simulations were performed with fixed numbers of N_c = 25 cell layers, N_f = 5 extracellular compartments per cell, N_{xin} = 78 intracellular metabolites per cell and N_{xout} = 3 extracellular metabolites resulting in an ODE system of $N_c \cdot N_{xin} + N_c \cdot N_f \cdot N_{xout} + N_{xout}$ = 2328 equations. The model was solved using LIMEX 4.2 with banded Jacobian techniques with absolute tolerance of $1E^{-6}$ and relative tolerance of $1E^{-3}$.

2.4 Strategies of energy production

Different strategies of ATP production were implemented by varying the relative capacities of GLY $\Phi_{GLY}(i)$ and OXP $\Phi_{OXP}(i)$ of the individual cells. Static strategies are those where the capacities $\Phi_{GLY}(i) = \Phi_{GLY}$ and $\Phi_{OXP}(i) = \Phi_{OXP}$ are independent of the location of the cell, whereas for adaptive strategies the metabolic capacities $\Phi_{GLY}(i)$ and $\Phi_{OXP}(i)$ vary with increasing distance from the blood vessel and towards the tumor core. As a boundary condition for all strategies, the total capacity of ATP production was assumed to be constant ($\Phi_{GLY}(i) + \Phi_{OXP}(i) = \Phi_{TOT}(i)$) and ATP consumption assumed to be identical for all cells. These assumptions were made to constrain the model to one effective parameter per cell describing the ATP-producing strategy via either GLY or OXP.

2.5 Viable tumor rim and oxygen consumption

The extension of the viable rim R_c (peripheral belt of viable cells) was defined by the condition that ATP exceeds a critical threshold value. This condition is in line with the observed decrease of ATP from the viable rim towards the tumor core [12, 23] and previous work modeling the viable rim by critical ATP levels [24]. The viable rim ranges to cell i meeting the conditions

$$atp_c = 0.1\ mM$$

$$atp^{i} \geq atp_c \wedge atp^{i+1} < atp_c$$

$$R_c = d_{cell} \cdot i$$

The oxygen consumption in the viable rim was calculated as the sum of oxygen consumption of all cells in the viable rim. The relative oxygen consumption was normalized relative to the maximal oxygen consumption under conditions of minimal glucose supply of 0.8 mM and maximal oxygen supply of 120 mmHg in the supporting vessel.

3 Results

First, we validated our model by comparing simulation results with data on pO_2 profiles, the thickness of the viable rim and oxygen consumption rates determined at various external glucose and oxygen concentrations in mouse breast-cancer spheroids. We then tested distinct metabolic strategies (static and adaptive) of energy production by varying the GLY and OXP capacities of the cells (Fig. 3). Finally, gradients in cellular energy metabolism, of glucose, lactate and oxygen within the tumor tissue (Fig. 4), pO_2 profiles, data for the thickness of the viable rim and oxygen consumption under various external glucose and oxygen availability (Fig. 5) were simulated with the best-fit model of zonated energy metabolism.

3.1 Warburg effect and metabolic reprogramming

The concentration gradients of nutrients and oxygen between the blood vessel and the tumor core depend strongly on the mode of ATP production (either GLY or OXP) of the cells. Therefore, various strategies of energy production with varying contributions of these pathways to ATP production were evaluated. Static strategies were compared to an adaptive strategy with increasing GLY and decreasing OXP from the blood vessel towards the hypoxic tumor core (Fig. 3A).

In contrast to normal tissues that produce around 90% of their ATP via OXP with GLY accounting for the remaining 10%, in many tumors over 50% of the cellular energy is produced in GLY [14, 25]. In line with these observations, the experimental data for pO_2 profiles (Figs. 3B and 3C), of the viable rim (Fig. 3D) and oxygen consumption (Fig. 3E) could only be reproduced under the assumption of a high glycolytic capacity amounting to more than 50% of total ATP production. Intriguingly, even the cells in layers close to the supporting blood vessel, having enough oxygen available, required high glycolytic capacity to explain the observed drops in oxygen towards the tumor core. Consequently, only a fraction of the pyruvate produced in GLY was completely oxidized in the TCA cycle

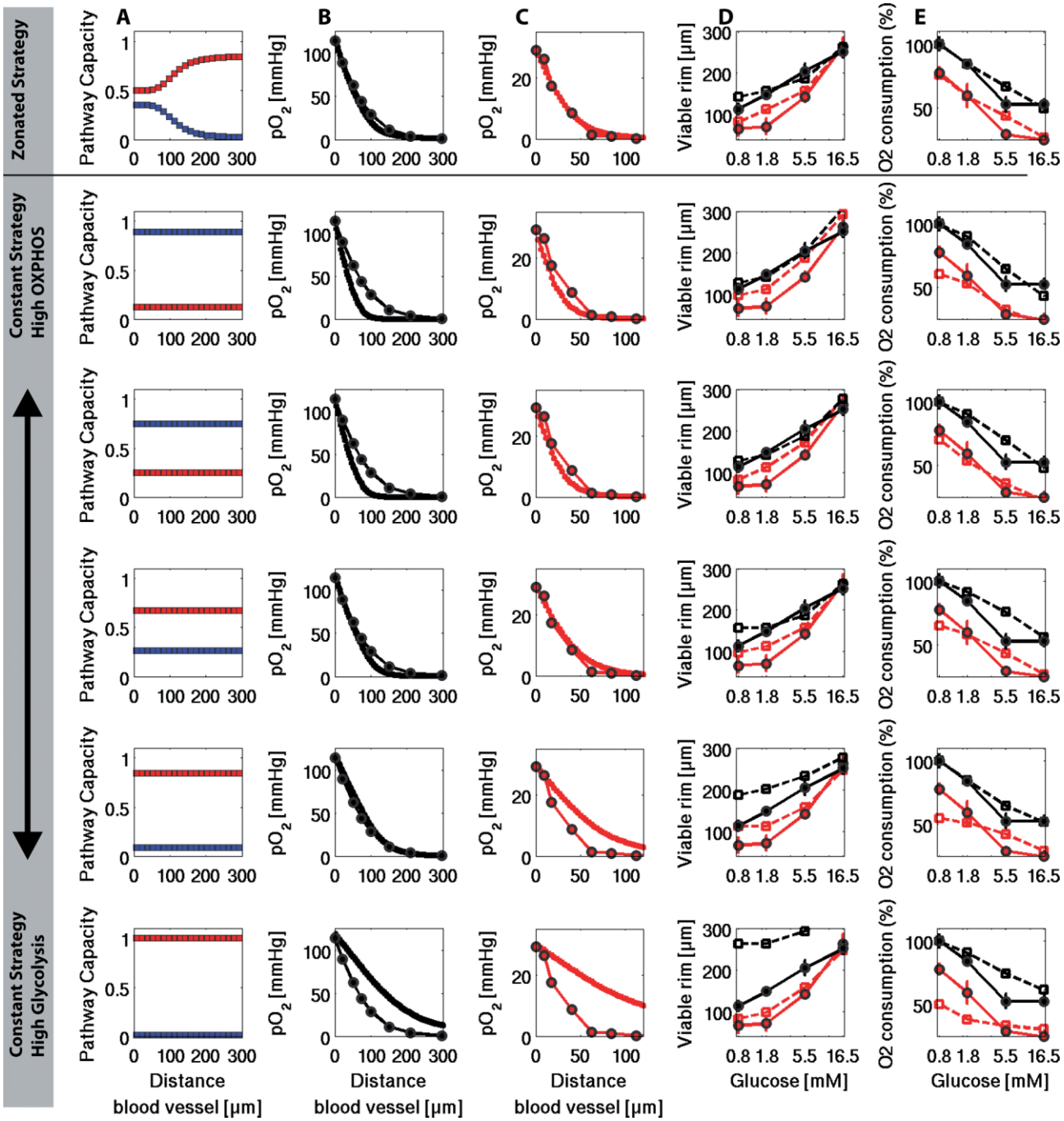

Figure 3. Metabolic strategies in tumor energy metabolism. (**A**) Metabolic strategy of energy production of the tumor cells with increasing distance from the blood vessel to the tumor core. Glycolytic capacity for ATP production (Φ_{GLY}) is depicted in blue, capacity of ATP production via OXP (Φ_{OXP}) in red. Static strategies assume identical capacities of the two pathways, whereas in the zonated strategy Φ_{GLY} and Φ_{OXP} are variable. Various static strategies with increasing glycolytic capacity from top to bottom were compared to the zonated strategy. (**B, C**) Two representative pO_2 profiles in EMT6/Ro spheroids grown under different external oxygen and glucose conditions (round, grey borders) [21] and the respective model simulations for the measured oxygen concentrations at the spheroid surface of (**B**) 120 mmHg oxygen for 20% oxygen at 1.8 mM glucose (black) and (**C**) 30 mmHg oxygen for 5% oxygen at 0.8 mM glucose (red). (**D**) Thickness of the viable rim (mean ± SD, n = 15–25) in EMT6/Ro spheroids cultured in media with four different glucose concentrations and 20% oxygen (black, solid) and 5% oxygen (red, solid) [21] and the respective model simulations for high (black, dashed) and low oxygen (red, dashed). The experimentally determined viable rim is based on histological characterization; the simulated viable rim is defined by the ATP level falling below a critical threshold (see Sect. 2). (**E**) Relative volume-related oxygen consumption rates (mean ± SE, n = 15–25) in the viable rim of EMT6/Ro spheroids cultured in media with four different glucose concentrations and 20% oxygen (black, solid) and 5% oxygen (red, solid) from [21] and the respective model simulations under high (black, dashed) and low pO_2 (red, dashed).

Biotechnol. J. 2013, 8, 1058–1069

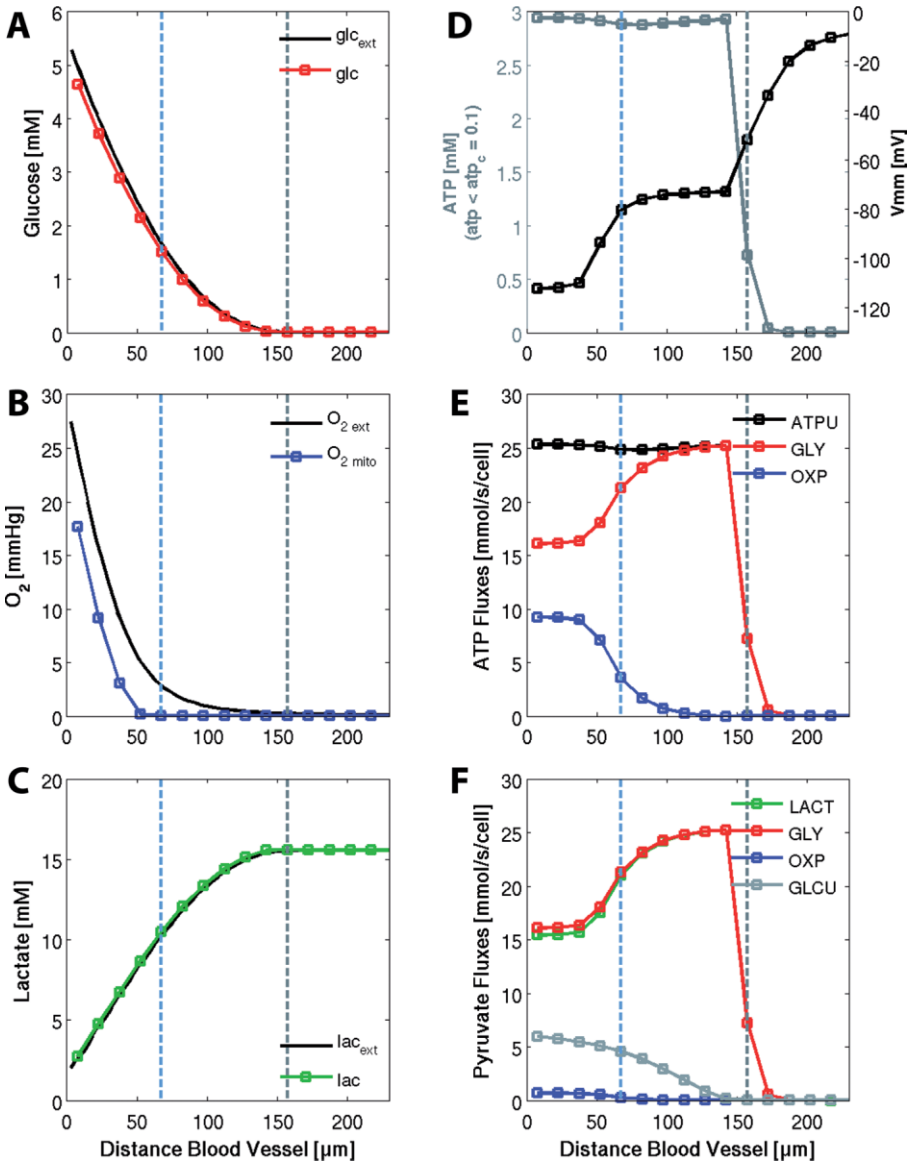

Figure 4. Metabolic gradients and energetic zonation. Steady-state solution of extracellular metabolites and energy metabolism with increasing distance from the supplying blood vessel at blood concentrations of 5.5 mM glucose, 30 mmHg oxygen and 1.4 mM lactate. Simulations were performed with zonated capacities for ATP production with increasing capacity for GLY Φ_{GLY} and decreasing capacity for OXP Φ_{GOXP} towards the tumor core (see Fig. 3A). The begin of the hypoxic tumor region is marked by the blue dashed line indicating the first cell with O_{2ext} 1 mmHg, whereas the energetically critical tumor region is marked by the grey dashed line indicating the last cell with ATP ≥ 0.1 mM. (**A**) Decline of glucose with increasing distance from the blood vessel. (**B**) Decline in oxygen with increasing distance from the blood vessel. (**C**) Elevation of lactate with increasing distance from the blood vessel. (**D**) Cellular energy state measured via ATP levels and mitochondrial membrane potential V_{mm}. With increasing distance from the blood vessel ATP levels decline and the mitochondrial membrane potential increases, resulting in a drop in the energetic state towards the tumor core. (**E**) ATP use (ATPU) and contribution of OXP and GLY to ATP production. (**F**) Pyruvate fluxes with increasing distance from the blood vessel. The pyruvate formed by GLY is either exported as lactate (MCT), or fully oxidized in the TCA cycle and OXP.

and OXP, resulting in high rates of lactate production even in the presence of sufficiently high oxygen concentrations, the so-called aerobe GLY or Warburg effect.

Oxygen becomes a limiting substrate for OXP if its concentration drops below 0.5% (~3 mmHg) [26]. On the other hand, oxygen is required for numerous non-respiratory purposes as, for example, hydroxylases [27], protein disulphide isomerases [28] and histone demethylases [29]. This non-mitochondrial oxygen consumption accounts for up to 10–30% of total cellular energy consumption [30, 31] and is essential for sterol synthesis and oxidative protein folding, the processes involved in proliferation. Therefore, too low oxygen concentrations could be one of the limiting factors for tumor growth [14] not only because of ceasing OXP, an idea already brought forward almost 60 years ago by Thomlinson and Gray [32]. By switching energy production in large parts of the tumor from OXP to GLY oxygen becomes accessible in more distant regions from the blood vessel (Figs. 3B and 3C) and is available for non-energy-producing cellular processes requiring oxygen. Hence, decreasing OXP and concomitantly increasing GLY, enables the tumor to enlarge the region where oxygen concentrations are still high enough to drive essential non-respiratory oxygen-consuming reactions.

3.2 Zonation of energy metabolism

Besides the reprogramming of tumor metabolism to high glycolytic capacities resulting in the Warburg effect, an additional level of complexity is introduced in the regulation of metabolism via the modulation of pathway capac-

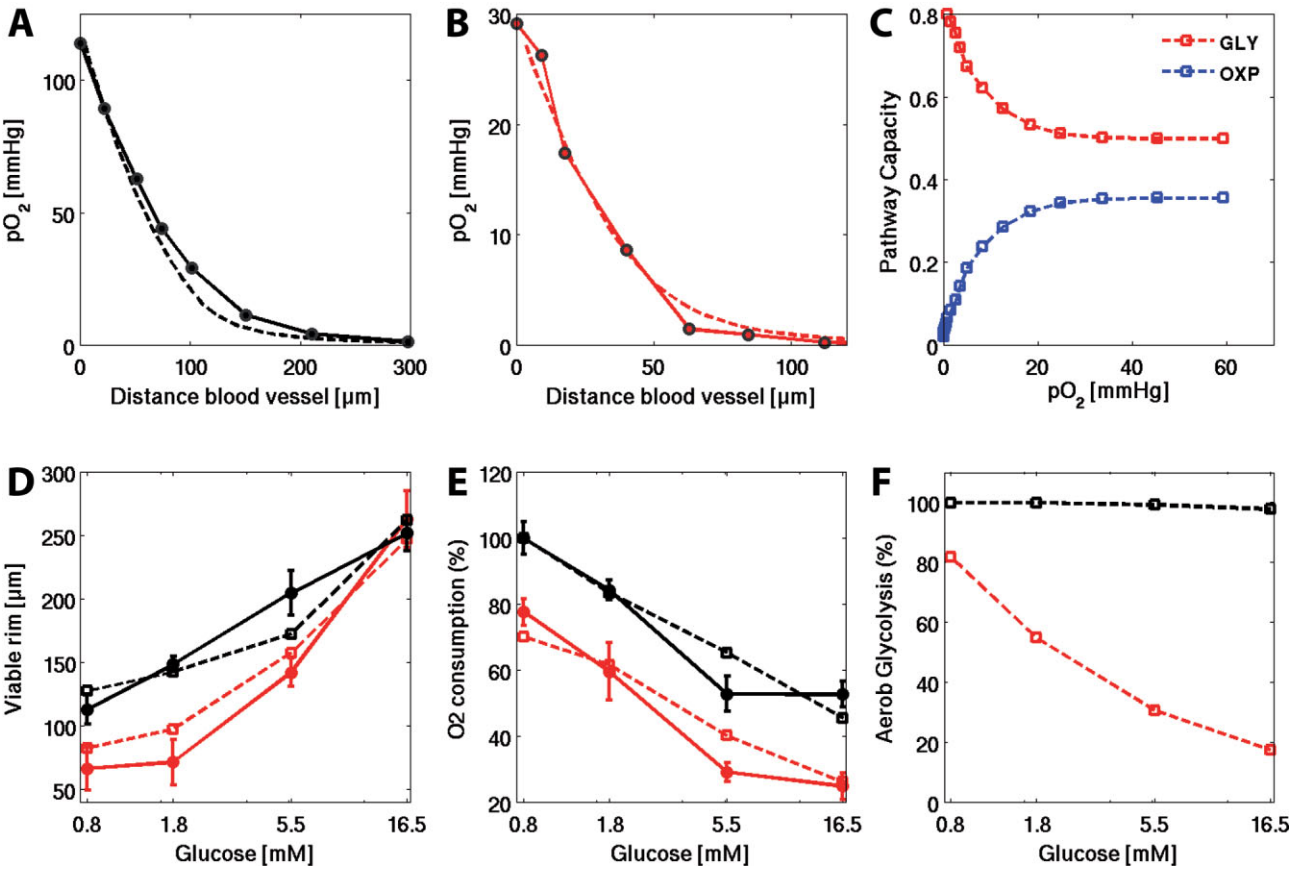

Figure 5. Zonated metabolism. (**A** and **B**) Two representative pO_2 profiles in EMT6/Ro spheroids grown under different external oxygen and glucose conditions (round, grey borders) [21] and the respective model simulations (dashed) for the measured oxygenconcentrations at the spheroid surface of (**A**) 120 mmHg oxygen for 20% oxygen at 1.8 mM glucose and (**B**) 30 mmHg oxygen for 5% oxygen at 0.8 mM. (**C**) Dependency of the capacities for GLY and OXP from the mean tissue oxygen concentrations for the simulated blood glucose and oxygen concentrations. Glycolytic capacity for ATP production increases, whereas capacity for OXP decreases with increasing hypoxia. (**D**) Viable rim thickness (mean ± SD, n = 15–25) in EMT6/Ro spheroids cultured in media with four different glucose concentrations and 20% oxygen (black, solid) and 5% oxygen (red, solid) [21] and the respective model simulations for high (black, dashed) and low oxygen (red, dashed). (**E**) Relative volume-related O_2 consumption rates (mean ± SE, n = 15–25) in the viable rim of EMT6/Ro spheroids cultured in media with four different glucose concentrations and media with high (black, solid) and low pO_2 (red, solid) from [21] and the respective model simulations under high (black, dashed) and low pO_2 (red, dashed). (**F**) Fraction of aerobe GLY under varying glucose and oxygen concentrations calculated as quotient of aerobic GLY/total GLY within the viable rim.

ities depending on available oxygen and glucose concentrations within the tumor tissue. In line with this idea, the best fit of the experimental data was achieved by assuming an energy metabolism with zonated pathway capacities comprising increased GLY and concomitant decrease in OXP from the blood vessel towards the tumor core under high glycolytic capacity (Fig. 3). This observation is supported by the reported progressive up-regulation of the glycolytic proteins from the surface layer towards the hypoxic cells and the inner necrotic core in tumor spheroids [13]. In the hypoxic region and necrotic core or both 8 out of 12 glycolytic enzymes were up-regulated, and none was down-regulated. Interestingly, static strategies with similar mean glycolytic capacity as used in simulations with adaptive strategies performed also well in fitting the data. Despite constant capacities for GLY and OXP, an intrinsic zonation of the energy metabolism is enforced by the tissue gradients of glucose, lactate and oxygen, resulting in a down-regulation of GLY due to glucose depletion and the limitation of OXP due to oxygen depletion in the hypoxic regions. The actual flux through GLY and OXP depends strongly on the available metabolite concentrations and therefore may become substrate-limited even at high pathway capacities.

Due to gradients of nutrients (glucose), waste products (lactate) and oxygen, the metabolic conditions become more and more challenging with increasing distance from the blood vessel, resulting in metabolically and energetically heterogeneous cell populations. A representative model simulation with zonated energy metabolism (5.5 mM glucose, 30 mmHg oxygen, 1.4 mM lactate) is given in Fig. 4, depicting the resulting steady-state ener-

getic and metabolic gradients. The model reproduces the typically observed decline in oxygen from the blood vessel towards the tumor core (Fig. 4B) [21, 22, 33] due to oxygen consumption in oxidative energy production (OXP, Fig. 4E). Glucose concentration declines towards the tumor core (Fig. 4A); the sugar is either used for glycolytic ATP production (GLY, Fig. 4E) or basic glucose usage (GLCU, Fig, 4F), which accounts for around 20% of the glucose taken up. This basal glucose consumption accounts for numerous essential cellular processes, e.g. synthesis of riboses for nucleotide synthesis, NADPH production via oxidative pentose phosphate pathway and synthesis of fatty acids and cholesterol from acetyl-CoA [15]. Lactate accumulates towards the tumor core (Fig. 4C) due to high glycolytic activity even under aerobic conditions. The energy state of the cells, measured in terms of ATP concentration and the mitochondrial membrane potential V_{mm} is progressively deteriorated towards the hypoxic region and becomes critical when glucose is depleted (Fig. 4D). The ATP production via GLY accounts for around 60% of total ATP production close to the blood vessel, with the remaining 40% from OXP, with glycolytic ATP production increasing to 100% in the hypoxic region. A large heterogeneity in glycolytic contribution exists between different tumor cell lines and tumor types. A glycolytic ATP contribution of 60% under normoxia, a value also estimated by Warburg [25], lies at the upper end of reported values (hepatoma Novicoff 64% and mouse ascites cancer 55%), compared to for instance 29–34% of glycolytic ATP production in MCF-7 breast cancer cells and Morris hepatoma 7777 cells and only around 10% for many fast-growing cell lines [34, 35].

The flux of pyruvate to OXP is minimal compared to the pyruvate generated in GLY and exported as lactate (Fig. 4F). The largest amount of pyruvate is directly exported under aerobic conditions because the high thermodynamic efficiency of OXP entails a small amount of pyruvate to be sufficient to meet the ATP demand.

3.3 Model validation and virtual histology

The zonated model of energy metabolism reproduces experimental data for oxygen profiles (Figs. 5A and 5B), viable rim thickness (Fig. 5D) and oxygen consumption (Fig. 5E) for a wide range of glucose and oxygen concentrations in mouse breast-carcinoma spheroids (EMT6/Ro) [21]. The viable rim thickness increases with increasing glucose and oxygen concentrations, whereas the size of the necrotic core increases with decreasing glucose concentration in the medium in agreement with measurements [21, 36, 37].

Based on calculated metabolite profiles in the extracellular space we can define four distinct metabolic regions: (i) A well-supplied region adjacent to the blood vessel with relatively high concentrations of oxygen and glucose harboring proliferating cells; (ii) an intermediate region with decreasing oxygen and glucose levels; (iii) an inner area of hypoxic cells relying almost exclusively on GLY; (iv) an inner necrotic core with critical drop of the energy state. This metabolic heterogeneity is in line with the histologically observed layers in tumor spheroids from the outer layers towards the core [13], with four to five lines of proliferating cells followed by quiescent and hypoxic cells and an inner necrotic tumor core [12].

3.4 Oxygen-dependent regulation of zonated energy metabolism

Hypoxia is as an important effector of gene and protein expression and many proteins of GLY are known HIF-1 target genes [14, 38]. The adaptation to hypoxia by an increase in glycolytic capacity and simultaneous decline in OXP is a plausible mechanism to adapt energy metabolism to ambient oxygen concentrations. Therefore, we were interested in the dose-response relationship between extracellular pO_2 and the relative share of OXP and GLY capacities (Fig. 5C). The model predicts the adaptation of the capacities of OXP and GLY to saturate around 30 mmHg with a half-activation of around ~10 mmHg. These values are in line with average pO_2 of normal tissues usually exceeding 20 mmHg [39] and an increase in the expression of many HIF-1-regulated genes when oxygen levels drop below 10 mmHg [40]. Hence, our model simulation lend further support to the concept that HIF-1-mediated control of enzyme activities represents a key mechanism to achieve zonated energy metabolism characterized by a shift of energy production to increased GLY and decreased mitochondrial function (OXP) [14].

4 Discussion

Our model-based study underlines the importance of metabolism as one of the newly emerging hallmarks of cancer [6]. The presented model predicts a strong metabolic reprogramming of cancer-energy metabolism towards high glycolytic capacity compared to normal tissues. Consequently, the tumor as a whole clearly displays the hallmark of the so-called Warburg effect, i.e. a high rate of glucose consumption and lactate production in the presence of sufficiently high levels of oxygen. The assumption of a zonated energy metabolism consisting in an increasing glycolytic capacity and concomitant decreasing capacity of OXP towards the hypoxic tumor core resulted in better fit of the experimental data compared to all other static strategies tested. On top of a high basal glycolytic capacity, tumor cells appear to be metabolically reprogrammed depending on the actual oxygen concentration in the tissue with HIF-1 being a crucial player in adapting the pathway capacities of GLY and OXP.

Clear limitations in the utilized metabolic model of tumor energy metabolism exist: (i) The presented study concentrated on tumor-energy metabolism with glucose as main carbon source not including glutamine, which plays an important role for proliferating cells and in tumor metabolism [41]. Glutamine can either be metabolized oxidatively after entering the TCA cycle as alpha-ketoglutarate, playing an important role as anaplerotic substrate, or can be metabolized reductively via the reverse isocitrate dehydrogenase reaction to provide glutamine-derived citrate for fatty acid synthesis [42]. Recent findings show that reductive glutamine metabolism becomes especially important under hypoxic conditions [43, 44] or in cells with defective mitochondria [45], resulting in a switch from glucose-derived to glutamine-derived citrate. Furthermore, glutamine can be involved in NADPH metabolism and as a source of lactate. Future work has to incorporate glutamine metabolism for modeling the interplay between glucose and glutamine as carbon and energy sources under varying oxygen conditions. (ii) A prerequisite for tumor-cell proliferation is the synthesis of macromolecules, including nucleotides, lipids and proteins from precursors, all processes closely linked to the energy metabolism. The presented model is limited to central energy metabolism not including these anabolic pathways, which will also influence the actual ATP demand of the cells, depending on their proliferation state. (iii) The model of energy metabolism was designed for neuronal tissues and is not adapted to the isoenzyme expression patterns of tumor metabolism, which can have strong regulatory implications for the analyzed tumor-energy metabolism.

The blood supply to tumors is spatially heterogeneous due to impaired tumor vascularization. This results in the existence of chronically hypoxic tumor regions. Moreover, temporal fluctuations of blood supply reported for tumors may give rise to cyclic phases of hypoxia [46, 47] and of nutrient availability, defining highly fluctuating and heterogeneous metabolic tumor microenvironments [23]. As a result, most tumors contain both highly perfused areas, which are rapidly growing, and areas with impaired perfusion, associated with necrosis. The strong selective pressure on mutagenic cancer cells to cope with these heterogeneities could select for cells with high basal glycolytic capacity [57]. These cells could survive and even proliferate in the front region in temporary phases of hypoxia and be better suited to cope with these heterogeneities and the major gradients of critical metabolites such as oxygen, glucose, lactate, as well as other nutrients like glutamate, hormones and growth factors – a microevolution driven by challenging metabolic conditions.

Possible future applications of the presented model are simulations of the effect of these spatio-temporal fluctuations on the tumor energy metabolism, the viable rim and oxygen consumption or the in silico evaluation of the metabolic effects of inhibitors of GLY or OXP [48, 49]. Metabolic zonation not only plays an important role in cancer, but also in normal tissue function, for instance in the liver [1, 2]. The presented framework of tissue-scale modeling by integration of single-cell kinetic models with models of extracellular transport can easily be adapted to model the zonated metabolism of other tissues, e.g. of the liver displaying a strong metabolic zonation of hepatocytes along liver sinusoids [1, 2]. An intriguing question to be addressed by such a zonated metabolic model of hepatic sinusoids pertains to the relative role of periportal and perivenous hepatocytes in the regulation of the blood glucose level [51].

This work was supported by the Federal Ministry of Education and Research (BMBF, Germany) within the Virtual Liver Network (VLN grant number 0315741). Special thanks to Dr. Rainald Ehrig for helping with the implementation in LIMEX and optimization of the numerical solution methods as well as to Thomas Dierkes and Susanna Röblitz from the department of numerical analysis and modeling at the Konrad Zuse Zentrum for Informationstechnik Berlin (ZIB).

The authors declare no commercial or financial conflict of interest.

5 References

[1] Jungermann, K., Kietzmann, T., Zonation of parenchymal and nonparenchymal metabolism in liver. *Annu. Rev. Nutr.* 1996, *16*, 179–203.

[2] Jungermann, K., Kietzmann, T., Role of oxygen in the zonation of carbohydrate metabolism and gene expression in liver. *Kidney Int.* 1997, *51*, 402-412.

[3] Gebhardt, R., Metabolic zonation of the liver: Regulation and implications for liver function. *Pharmacol. Ther.* 1992, *53*, 275–354.

[4] Torre, C., Perret, C., Colnot, S., Molecular determinants of liver zonation. *Prog. Mol. Biol. Transl. Sci.* 2010, *97*, 127–150.

[5] Gebhardt, R., Hovhannisyan, A., Organ patterning in the adult stage: The role of Wnt/beta-catenin signaling in liver zonation and beyond. *Dev. Dyn.* 2010, *239*, 45–55.

[6] Hanahan, D., Weinberg, R. A., Hallmarks of cancer: The next generation. *Cell* 2011, *144*, 646–674.

[7] Wilson, W. R., Hay, M. P., Targeting hypoxia in cancer therapy. *Nat. Rev. Cancer* 2011, *11*, 393–410.

[8] Ruan, K., Song, G., Ouyang, G., Role of hypoxia in the hallmarks of human cancer. *J. Cell. Biochem.* 2009, *107*, 1053–1062.

[9] Jain, R. K., Normalization of tumor vasculature: An emerging concept in antiangiogenic therapy. *Science* 2005, *307*, 58–62.

[10] Pries, A. R., Cornelissen, A. J. M., Sloot, A. A., Marlene Hinkeldey, M. et al., Structural adaptation and heterogeneity of normal and tumor microvascular networks. *PLoS Comput. Biol.* 2009, *5*, e1000394.

[11] Semenza, G. L., Tumor metabolism: Cancer cells give and take lactate. *J. Clin. Invest.* 2008, *118*, 3835–3837.

[12] Sutherland, R. M., Cell and environment interactions in tumor microregions: The multicell spheroid model. *Science* 1988, *240*, 177–184.

[13] McMahon, K. M., Volpato, M., Chi, H. Y., Musiwaro, P. et al., Characterization of changes in the proteome in different regions of 3D multicell tumor spheroids. *J. Proteome Res.* 2012, *11*, 2863–2875.
[14] Denko, N. C., Hypoxia, HIF1 and glucose metabolism in the solid tumour. *Nat. Rev. Cancer* 2008, *8*, 705–713.
[15] Herling, A., König, M., Bulik, S., Holzhütter, H.-G., Enzymatic features of the glucose metabolism in tumor cells. *FEBS J.* 2011, *278*, 2436–2459.
[16] Kim, J. W., Tchernyshyov, I., Semenza, G. L., Dang, C. V., HIF-1-mediated expression of pyruvate dehydrogenase kinase: A metabolic switch required for cellular adaptation to hypoxia. *Cell metabolism* 2006, *3*, 177–185.
[17] Papandreou, I., Cairns, R. A., Fontana, L., Lim, A. L., Denko, N. C., HIF-1 mediates adaptation to hypoxia by actively downregulating mitochondrial oxygen consumption. *Cell metabolism* 2006, *3*, 187–197.
[18] Zhang, H., Gao, P., Fukuda, R., Kumar, G. et al., HIF-1 inhibits mitochondrial biogenesis and cellular respiration in VHL-deficient renal cell carcinoma by repression of C-MYC activity. *Cancer Cell* 2007, *11*, 407–420.
[19] Marín-Hernández, A., Gallardo-Pérez, J. C., Rodríguez-Enríquez, S., Encalada, R.. et al., Modeling cancer glycolysis. *Biochim. Biophys. Acta* 2010.
[20] Berndt, N., Bulik, S., Holzhutter, H. G., Kinetic Modeling of the Mitochondrial energy metabolism of neuronal cells: The impact of reduced alpha-Ketoglutarate dehydrogenase activities on ATP production and generation of reactive oxygen species. *Int. J. Cell Biol.* 2012, *2012*, 757594.
[21] Mueller-Klieser, W., Freyer, J. P., Sutherland, R. M., Influence of glucose and oxygen supply conditions on the oxygenation of multicellular spheroids. *Br. J. Cancer* 1986, *53*, 345–353.
[22] Mueller-Klieser, W., Method for the determination of oxygen consumption rates and diffusion coefficients in multicellular spheroids. *Biophys. J.* 1984, *46*, 343–348.
[23] Vaupel, P., Kallinowski, F., Okunieff, P., Blood flow, oxygen and nutrient supply, and metabolic microenvironment of human tumors: A review. *Cancer Res.* 1989, *49*, 6449–6465.
[24] Bertuzzi, A., Fasano, A., Gandolfi, A., Sinisgalli, C., Necrotic core in EMT6/Ro tumour spheroids: Is it caused by an ATP deficit? *J. Theor. Biol.* 2010, *262*, 142–150.
[25] WARBURG, O., On the origin of cancer cells. *Science* 1956, *123*, 309–314.
[26] Chandel, N., Budinger, G. R., Kemp, R. A., Schumacker, P. T., Inhibition of cytochrome-c oxidase activity during prolonged hypoxia. *Am. J. Physiol.* 1995, *268*, L918–925.
[27] Hagen, T., Taylor, C. T., Lam, F., Moncada, S., Redistribution of intracellular oxygen in hypoxia by nitric oxide: Effect on HIF1alpha. *Science* 2003, *302*, 1975–1978.
[28] Tu, B. P., Weissman, J. S., The FAD- and O(2)-dependent reaction cycle of Ero1-mediated oxidative protein folding in the endoplasmic reticulum. *Mol. Cell.* 2002, *10*, 983–994.
[29] Forneris, F., Binda, C., Vanoni, M. A., Mattevi, A., Battaglioli, E., Histone demethylation catalysed by LSD1 is a flavin-dependent oxidative process. *FEBS Lett.* 2005, *579*, 2203–2207.
[30] Herst, P. M., Berridge, M. V., Cell surface oxygen consumption: A major contributor to cellular oxygen consumption in glycolytic cancer cell lines. *Biochim. Biophys. Acta* 2007, *1767*, 170–177.
[31] Rosenfeld, E., Beauvoit, B., Rigoulet, M., Salmon, J. M., Non-respiratory oxygen consumption pathways in anaerobically-grown Saccharomyces cerevisiae: Evidence and partial characterization. *Yeast* 2002, *19*, 1299–1321.
[32] Thomlinson, R. H., Gray, L. H., The histological structure of some human lung cancers and the possible implications for radiotherapy. *Br. J. Cancer* 1955, *9*, 539–549.
[33] Helmlinger, G., Yuan, F., Dellian, M., Jain, R. K., Interstitial pH and pO2 gradients in solid tumors in vivo: High-resolution measurements reveal a lack of correlation. *Nat. Med.* 1997, *3*, 177–182.
[34] Zu, X. L., Guppy, M., Cancer metabolism: Facts, fantasy, and fiction. *Biochem. Biophys. Res. Comm.* 2004, *313*, 459–465.
[35] Moreno-Sanchez, R., Rodriguez-Enriquez, S., Marin-Hernandez, A., Saavedra, E., Energy metabolism in tumor cells. *FEBS J.* 2007, *274*, 1393–1418.
[36] Luk, C. K., Sutherland, R. M., Nutrient modification of proliferation and radiation response in EMT6/Ro spheroids. *Int. J. Radiat. Oncol. Biol. Phys.* 1987, *13*, 885–895.
[37] Casciari, J. J., Sotirchos, S. V., Sutherland, R. M., Glucose diffusivity in multicellular tumor spheroids. *Cancer Res.* 1988, *48*, 3905–3909.
[38] Iyer, N. V., Kotch, L. E., Agani, F., Leung, S. W. et al., Cellular and developmental control of O2 homeostasis by hypoxia-inducible factor 1 alpha. *Genes & Development* 1998, *12*, 149–162.
[39] Braun, R. D., Lanzen, J. L., Snyder, S. A., Dewhirst, M. W., Comparison of tumor and normal tissue oxygen tension measurements using OxyLite or microelectrodes in rodents. *AJP. Heart and Circulatory Physiology* 2001, *280*, H2533–2544.
[40] Semenza, G. L., Targeting HIF-1 for cancer therapy. *Nat. Rev. Cancer* 2003, *3*, 721–732.
[41] Daye, D., Wellen, K. E., Metabolic reprogramming in cancer: Unraveling the role of glutamine in tumorigenesis. *Semin. Cell Dev. Biol.* 2012, *23*, 362–369.
[42] DeBerardinis, R. J., Mancuso, A., Daikhin, E., Nissim, I. et al., Beyond aerobic glycolysis: Transformed cells can engage in glutamine metabolism that exceeds the requirement for protein and nucleotide synthesis. *Proc. Natl. Acad. Sci. USA* 2007, *104*, 19345–19350.
[43] Metallo, C. M., Gameiro, P. A., Bell, E. L., Mattaini, K. R. et al., Reductive glutamine metabolism by IDH1 mediates lipogenesis under hypoxia. *Nature* 2012, *481*, 380–384.
[44] Filipp, F. V., Scott, D. A., Ronai, Z. A., Osterman, A. L., Smith, J. W., Reverse TCA cycle flux through isocitrate dehydrogenases 1 and 2 is required for lipogenesis in hypoxic melanoma cells. *Pigment Cell Melanoma Res.* 2012, *25*, 375–383.
[45] Mullen, A. R., Wheaton, W. W., Jin, E. S., Chen, P. H. et al., Reductive carboxylation supports growth in tumour cells with defective mitochondria. *Nature* 2012, *481*, 385–388.
[46] Dewhirst, M. W., Cao, Y., Moeller, B., Cycling hypoxia and free radicals regulate angiogenesis and radiotherapy response. *Nat. Rev. Cancer* 2008, *8*, 425–437.
[47] Cárdenas-Navia, L. I., Mace, D., Richardson, R. A., Wilson, D. F., et al., The pervasive presence of fluctuating oxygenation in tumors. *Cancer Res.* 2008, *68*, 5812–5819.
[48] Mathupala, S. P., Metabolic targeting of malignant tumors: Small-molecule inhibitors of bioenergetic flux. *Recent Pat. Anti-cancer drug Discov.* 2011, *6*, 6–14.
[49] Marin-Hernandez, A., Gallardo-Perez, J. C., Lopez-Ramirez, S. Y., Garcia-Garcia, J. D. et al., Casiopeina II-gly and bromo-pyruvate inhibition of tumor hexokinase, glycolysis, and oxidative phosphorylation. *Arch. Toxicol.* 2012, *86*, 753–766.
[50] König, M., Bulik, S., Holzhütter, H. G., Quantifying the contribution of the liver to glucose homeostasis: A detailed kinetic model of human hepatic glucose metabolism. *PLoS Comput. Biol.* 2012, *8*, e1002577.
[51] Groebe, K., Erz, S., Mueller-Klieser, W., Glucose diffusion coefficients determined from concentration profiles in EMT6 tumor spheroids incubated in radioactively labeled L-glucose. *Adv. Exp. Med. Biol.* 1994, *361*, 619–625.
[52] Höber, R. (Ed.), *Physical Chemistry of Cells and Tissues*, The Blakiston company, 1947.
[53] Freeman, D. M., Sotak, C. H., Muller, H. H., Young, S. W., Hurd, R. E., A double quantum coherence transfer proton NMR spectroscopy

technique for monitoring steady-state tumor lactic acid levels in vivo. *Magn. Reson. Med.* 1990, *14*, 321–329.

[54] Pfeuffer, J., Lin, J. C., Delabarre, L., Ugurbil, K., Garwood, M., Detection of intracellular lactate with localized diffusion {1H-13C}-spectroscopy in rat glioma in vivo. *J. Magn. Reson.* 2005, *177*, 129–138.

[55] Grote, J., Susskind, R., Vaupel, P., Oxygen diffusivity in tumor tissue (DS-carcinosarcoma) under temperature conditions within the range of 20—40 degrees C. *Pflugers Arch.* 1977, *372*, 37–42.

[56] Vaupel, P., Effect of percentual water content in tissues and liquids on the diffusion coefficients of O2, CO2, N2, and H2. *Pflugers Arch.* 1976, *361*, 201–204.

[57] Shibata, D., Cancer. Heterogeneity and tumor history. *Science* 2012, *336*, 304–305.

[58] Ng, C. S., Waterton, J. C., Kundra, V., Brammer, D. et al., Reproducibility and comparison of DCE-MRI and DCE-CT perfusion parameters in a rat tumor model. *Technol. Cancer Res. Treatment* 2012, *11*, 279–288.

Special issue: *Metabolic Modeling and Simulation*. Modeling of cellular metabolism has been a major area of research for bioengineers and biomedical researchers alike. This Special Issue collects a series of articles on methods of metabolic modeling, modeling of human metabolism, modeling of microbial metabolism and modeling of bioprocesses. This cover is a visual representation of the essence of metabolic engineering. Image: © rolffimages – Fotolia.com.

Biotechnology Journal – list of articles published in the September 2013 issue.